Nonvolatile Ionic Modification of the Dzyaloshinskii-Moriya Interaction

L. Herrera Diez,[1,*] Y.T. Liu,[1] D.A. Gilbert,[2,3] M. Belmeguenai,[4] J. Vogel,[5] S. Pizzini,[5] E. Martinez,[6] A. Lamperti,[7] J.B. Mohammedi,[8] A. Laborieux,[1] Y. Roussigné,[4] A.J. Grutter,[2] E. Arenholtz,[9] P. Quarterman,[2] B. Maranville,[2] S. Ono,[10] M. Salah El Hadri,[11] R. Tolley,[11] E.E. Fullerton,[11] L. Sanchez-Tejerina,[12] A. Stashkevich,[4] S.M. Chérif,[4] A.D. Kent,[8] D. Querlioz,[1] J. Langer,[13] B. Ocker,[13] and D. Ravelosona[1]

[1] *Centre de Nanosciences et de Nanotechnologies, CNRS, Univ. Paris-Sud, Université Paris-Saclay, C2N—Palaiseau, 91120 Orsay cedex, France*

[2] *NIST Center for Neutron Research, National Institute of Standards and Technology, Gaithersburg, Maryland 20899, USA*

[3] *Department of Materials Science and Engineering, University of Tennessee, Knoxville, Tennessee 37919, USA*

[4] *Laboratoire des Sciences des Procédés et des Matériaux, CNRS-UPR 3407, Université Paris 13, Sorbonne Paris Cité, 93430 Villetaneuse, France*

[5] *Univ. Grenoble Alpes, CNRS, Institut Néel, 38000 Grenoble, France*

[6] *Departamento de Física Aplicada, Universidad de Salamanca, Plaza de la Merced s/n. 37008 Salamanca, Spain*

[7] *IMM-CNR, Unit of Agrate Brianza, Via C. Olivetti 2, 20864 Agrate Brianza (MB), Italy*

[8] *Department of Physics, New York University, New York, New York 10003, USA*

[9] *Advanced Light Source, Lawrence Berkeley National Laboratory, Berkeley, California 94720, USA*

[10] *Central Research Institute of Electric Power Industry, Yokosuka, Kanagawa 240-0196, Japan*

[11] *Center for Memory and Recording Research, University of California, San Diego, La Jolla, California 92093-0401, USA*

[12] *Dpto. Electricidad y Electronica, University of Valladolid, 47011 Valladolid, Spain*

[13] *Singulus Technology AG, Hanauer Landstrasse 103, 63796 Kahl am Main, Germany*

(Received 29 May 2019; revised manuscript received 7 August 2019; published 4 September 2019)

The possibility of tuning the Dzyaloshinskii-Moriya interaction (DMI) by electric (E)-field gating in ultrathin magnetic materials has opened up new perspectives in terms of controlling the stabilization of chiral spin structures. The most recent efforts have used voltage-induced charge redistribution at the interface between a metal and an oxide to modulate the DMI. This approach is attractive for active devices but tends to be volatile, making it energy-demanding, and it is limited by Coulomb screening in the metal. Here we demonstrate nonvolatile E-field manipulation of the DMI by ionic-liquid gating of $Pt/Co/HfO_2$ ultrathin films. The E-field effect on the DMI scales with the E-field exposure time, and we propose that it is linked to the migration of oxygen species from the HfO_2 layer into the Co and Pt layers and subsequent anchoring. This effect permanently changes the properties of the material, showing that E fields can be used not only for local gating in devices but also as a highly scalable materials design tool for postgrowth tuning of the DMI.

DOI: 10.1103/PhysRevApplied.12.034005

I. INTRODUCTION

Controlling magnetic states in ferromagnetic metals by electric (E) fields [1] is a promising route for lowering power consumption in spintronic devices. Lowering critical switching currents in magnetic tunnel junctions [2] and improving domain-wall motion in racetrack devices [3] by inducing E-field anisotropy modulations are among the most exciting possibilities. The Dzyaloshinskii-Moriya interaction (DMI) has also revealed itself as a key element in the design of novel spintronic devices, since it can induce the formation of chiral magnetic structures such as skyrmions and Néel-like domain walls [4]. Controlling the DMI by E fields is therefore of outstanding practical interest, since it could allow dynamic and local tuning of chiral spin structures.

E-field control of magnetic anisotropy and domain-wall (DW) dynamics through a pure charge-accumulation [5–9] or an ionic-motion mechanism [6,9–13] has been demonstrated, the nonvolatility of the ionic effects making them

*liza.herrera-diez@c2n.upsaclay.fr

particularly interesting for applications. E-field control of the DMI through volatile charge accumulation in Co-Fe-B/TaO_x [14] and Pt/Co/Pd [15] systems has been recently observed. In addition, a reported E-field-induced modulation of skyrmion bubble nucleation in Pt/Co/Al_2O_3 [16] indicates also a potential E-field effect on the DMI. In terms of ionic effects on the DMI, evidence has been shown indirectly in the form of ionic control of the spin Hall angle [17] in Pt/Co/GdO_x systems. However, a detailed characterization of the effects of E-field-induced ionics on the DMI and an assessment of the full potential of ionics in defining the magnitude of the DMI in a nonvolatile fashion is still lacking.

In this study, we present a nonvolatile and cumulative E-field-induced reduction of the DMI in Pt/Co(0.6 nm)/HfO_2/ionic-liquid (IL) gate devices which is accompanied by a spin-reorientation transition (SRT) from in-plane to perpendicular magnetic anisotropy (PMA). These E-field-induced changes are related to the migration of oxygen species from HfO_2 into the Co and Pt layers, producing gentle oxidation of the Co and important structural changes at the interfaces. Oxidation at the Co/HfO_2 interface is thought to be responsible for an increase (and subsequent decrease at long biasing times) in the PMA, while Co oxidation and ion recombination at the Pt/Co interface is thought to lead to a decoupling between the Pt and Co layers and, in turn, a weakening of the DMI.

It is worth noting that the liquid gate [18] can be removed after these nonvolatile effects have been induced, opening up the possibility of using E fields as a low-cost simple tool for material design.

II. MAGNETIZATION, PERPENDICULAR ANISOTROPY, AND DMI

Figure 1 shows a schematic view of the device, and hysteresis loops measured in a perpendicular magnetic field for an as-grown film (black line) and a film exposed to a gate voltage of −3 V (red line) for a duration of 1 min. A full SRT into a perpendicular magnetic-anisotropy state takes place and persists when the voltage and liquid gate are removed. All experiments are conducted in ambient conditions and the bias voltage (−3 V) is applied between the Pt layer and a top counterelectrode coated with transparent $InSnO_x$ (ITO) for 1–22 min. The resulting E-field at the surface of the film is approximately 0.6 GV/m (see the Supplemental Material [19] for more details). Figure 2 shows the evolution of the measured product $M_s \times t$ (circles), where M_s and t are the saturation magnetization and the film thickness, respectively. M_s is measured by superconducting quantum interference device (SQUID) magnetometry using out-of-plane magnetic-field ramps going up to saturation fields of 600 and 120 mT for the as-grown and biased samples, respectively. Straight lines are subtracted from all loops to correct for the diamagnetic

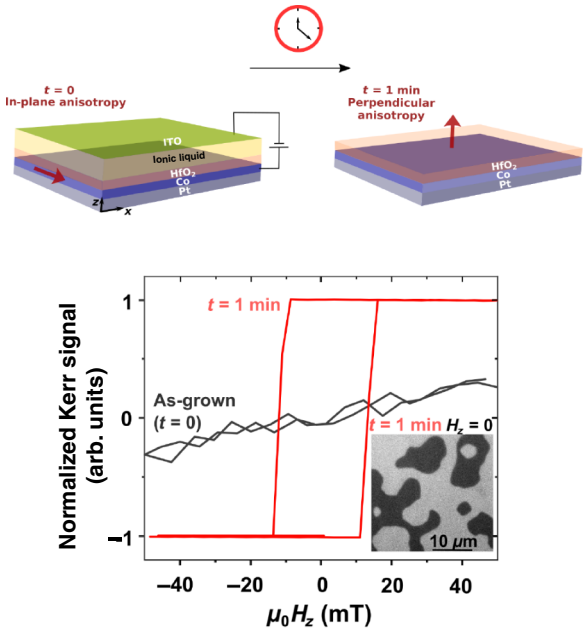

FIG. 1. Schematic of the Pt/Co/HfO_2 liquid gate device together with hysteresis loops measured in a perpendicular magnetic field before (black) and after (red) applying a gate voltage of −3 V for 1 min. The Kerr-microscopy image (inset) shows the domain pattern in the demagnetized state after the gate voltage application.

background. All of the film pieces are cleaved from the same wafer and have the same properties before E-field exposure. The anisotropy field $\mu_0 H_K$ measured by Brillouin light scattering (BLS) (filled squares) and SQUID (empty squares) as a function of the biasing time is also shown. $M_s \times t$ increases between 0 and 1 min, followed by a monotonic decrease. The trend in $\mu_0 H_K$ suggests a weakening of the perpendicular-magnetic-anisotropy constant K_{eff} ($\mu_0 H_K = 2K_{\text{eff}}/M_s$, considering a constant $t = 0.6$ nm; see the Supplemental Material [19]) beyond 4 min.

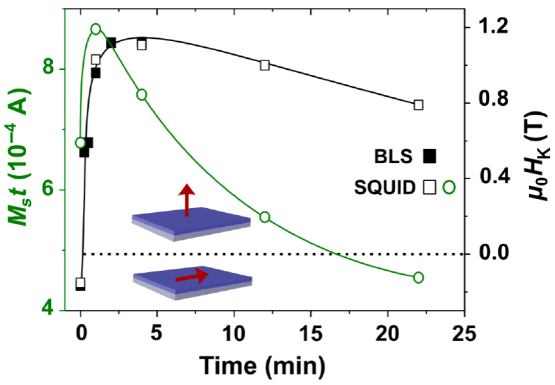

FIG. 2. (a) $M_s \times t$ (circles) and (b) $\mu_0 H_K$ (squares) as a function of the E-field biasing time. The lines are a guide to the eye.

The values of the strength of the DMI constant D measured by BLS are shown in Fig. 3(a) (filled symbols). These values are obtained by analyzing, under a saturating in-plane magnetic field, the frequency asymmetry ΔF of the BLS Stokes and anti-Stokes inelastic scattering peaks as a function of the wave vector k [20] shown in Fig. 3(b), a dependence governed by the following equation:

$$\Delta F = \frac{2\gamma}{\pi M_s} Dk, \tag{1}$$

where γ is the gyromagnetic ratio. The Stokes and anti-Stokes peaks for an as-grown film and a film biased for 1 min are shown in Figs. 3(c) and 3(d), respectively (see the Supplemental Material [19] for the full dataset). The solid lines correspond to a Lorenzian fitting of the peaks. The absolute DMI value shows a strong decrease between 0 and 1 min and tends to stabilize around $D = -0.3$ mJ/m^2 in the range between 2 and 4 min. These values are calculated using the measured $M_s \times t$ values presented in Fig. 2 (filled symbols) or an estimation based on the same dataset (empty symbols) and considering a nominal Co layer thickness of 0.6 nm. Potential E-field-induced variations in t are taken into account and do not modify these results significantly (see the Supplemental Material [19]). Reversing the E-field polarity or removing the ionic liquid from the samples does not recover the values of the DMI, M_s, or $\mu_0 H_K$, indicating that the induced changes are permanent and irreversible (see the Supplemental Material [19]). The total DMI variation presented here amounts to a factor of approximately 2.9 with respect to the initial value, which is significantly higher than the variations obtained by charge accumulation in both Co-Fe-B/TaO_x [14] and Pt/Co/Pd [15] systems, which are by factors of nearly 2.2 and 1.1, respectively.

III. MAGNETIC-DOMAIN-WALL MOTION

The value of the DMI can also be evaluated by measuring the asymmetry of magnetic-DW motion under the influence of simultaneous in-plane and out-of-plane magnetic fields [21,22] in the perpendicular-anisotropy regime. Typical Kerr-microscopy images of the asymmetric expansion of magnetic domains in in-plane fields ($\mu_0 H_X$), a signature of the presence of the DMI, in a film biased for 1 min are presented in Fig. 4(a). The velocity curves under $\mu_0 H_X$ for films biased for 1 and 4 min [Figs. 4(b) and 4(c), respectively] show minima at $\pm\mu_0 H_{\mathrm{DMI}}$ that are correlated with the magnitude of the DMI parameter D:

$$\mu_0 H_{\mathrm{DMI}} = \frac{D}{M_s \Delta}, \tag{2}$$

where $\Delta = \sqrt{A/K_{\mathrm{eff}}}$ is the domain-wall width parameter and A is the exchange stiffness constant [21] (see the Supplemental Material [19] for the full dataset). D values are

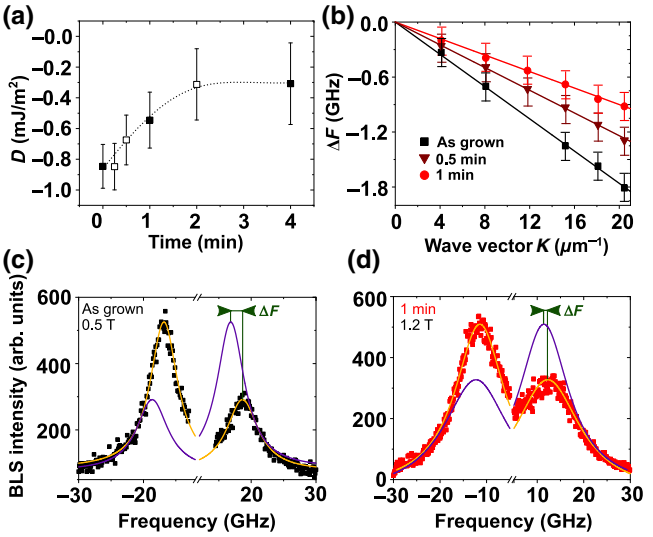

FIG. 3. (a) DMI constant D as a function of the biasing time; values calculated using estimated M_s values are shown as empty symbols. The dotted line is a guide to the eye. (b) Frequency asymmetry as a function of the wave vector, and linear fitting lines. BLS spectra at $k = 20$ μm^{-1} for the (c) as-grown and (d) 1-min-biased films. The solid lines correspond to a Lorenzian fitting.

calculated for biasing times of 1, 2, 4, and 12 min and are shown in Fig. 4(d). The value of A used in these calculations is determined by measuring the temperature dependence of the magnetic moment for as-grown, 1 min, and 4 min samples and evaluating the validity of the Bloch $T^{3/2}$ law [23,24] (see the Supplemental Material [19]). The values of A are shown in Fig. 4(e); they vary between 9 and 12 pJ/m, which are below the typical value used for thin films (16 pJ/m [25,26]). This difference can be attributed to the ultrathin nature of the magnetic film [23], which could contribute to a more pronounced influence of alloying with Pt; this has been shown to induce a decrease in A [26].

Although the D values measured by BLS and DW motion show a similar trend, the DW-motion measurements give higher values and a weaker dependence on the E field than those obtained by BLS. The origin of the discrepancies between these two sets of values remains an open question. Discrepancies between D values obtained by DW-motion experiments under in-plane fields and BLS have already been reported and attributed to the difference in the length scales probed by each technique [21] or to the limitations of a simplified model in more complex scenarios [27]. In this context, an inhomogeneous D in the film could be responsible for the discrepancy. Since the mechanism for the modulation of D in this study is related to a modification of the material, it cannot be ruled out that the E-field effect has an impact not only on the average value of D but also on its distribution across the sample, for example through preferential ionic accumulation in the vicinity of a defect, which could increase any discrepancy

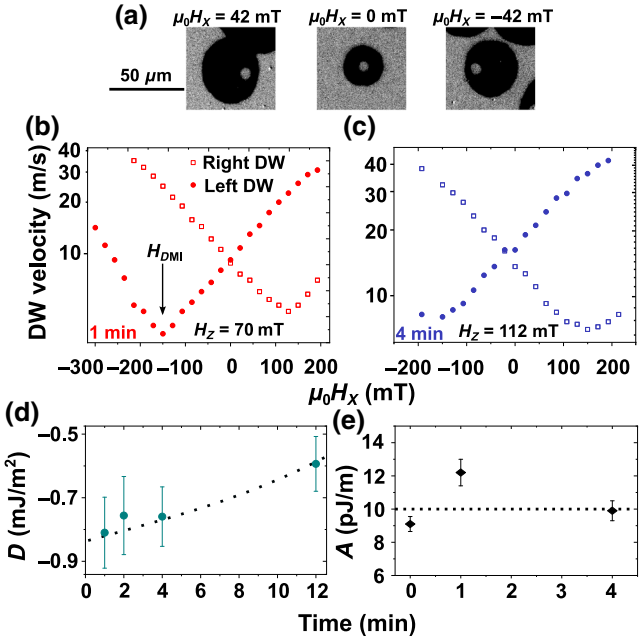

FIG. 4. (a) Kerr-microscopy images of domain expansion in the sample biased for 1 min under in-plane fields ($\mu_0 H_X$). Velocity curves as a function of $\mu_0 H_X$ from films biased for (b) 1 and (c) 4 min. (d) DMI parameter D extracted using the experimentally obtained values of A shown in (e). The lines are a guide to the eye.

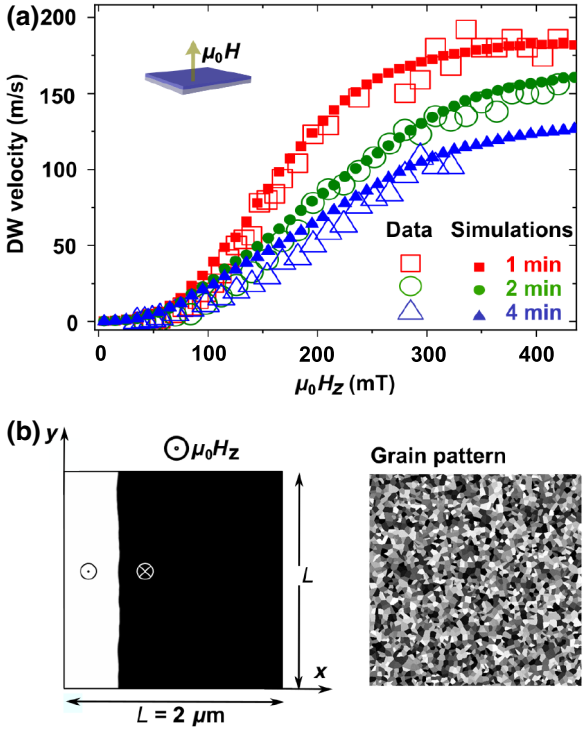

FIG. 5. (a) Experimental domain-wall velocity as a function of perpendicular magnetic field for films biased for 1, 2, and 4 min (open symbols), and micromagnetic simulations (filled symbols). (b) Granular structure used for the micromagnetic simulations.

between different measurement methods. Additionally, the calculation of D values from DW-motion measurements depends on the accuracy of the measured K_{eff} and A values, an uncertainty that is not present in the derivation of the D values by BLS and which could give rise to a discrepancy with the values obtained from DW motion.

Figure 5(a) shows the DW-velocity curves as a function of the perpendicular-magnetic-field strength obtained for biasing times of 1, 2, and 4 min (open symbols), indicating a strong reduction of the DW velocity consistent with the observed decrease in D. The curves do not show the typical dependence described by the one-dimensional model of DW motion [28], namely a strong decrease of the speed after the Walker field, followed by a linear increase with low mobility; instead, they show a saturation of the DW velocity at high magnetic fields. This feature, which has already been observed in a number of materials, including Pt/Co [25,29,30], has been attributed to instabilities of the internal structure of the DW above the Walker field, where the annihilation of vertical Bloch lines allows high velocities to be maintained after the Walker field [31].

Micromagnetic simulations conducted in order to better understand the mechanism behind the observed velocity reduction are also shown in Fig. 5(a) (filled symbols). The simulations are performed considering an area of 2 μm × 2 μm and a granular structure with a grain size of 20 nm and a dispersion of K_{eff}, M_s, and D in order to simulate disorder [see Fig. 5(b) and the Supplemental Material [19] for more details]. The simulated disorder introduced here is based on the typical grain-size values found in the literature for this type of material. Individual variations of the experimental parameters for each grain are introduced randomly in the range 0–20%, which has an average of 10%, also a typical value [27,32]. The simulations presented in Fig. 5(b) are obtained with values of D of 1.3, 1.05, and 0.74 mJ/m^2 for the samples biased for 1, 2, and 4 min, respectively, which are significantly higher than the D values obtained from either BLS or DW motion. Other studies in the literature [30] have shown that intermixing and disorder at the ferromagnetic-heavy-metal interface not only can lead to changes in D but also can have a large impact on the value of the DW-velocity plateau. A careful analysis of the impact of E-field-induced ionic motion on disorder is needed to complete the picture and better understand the discrepancies between the values of D obtained by different methods. Nevertheless, the decreasing trend in the DMI strength with respect to the exposure time is confirmed by all methods.

IV. STRUCTURAL ANALYSIS

In order to elucidate the mechanism behind the E-field-induced modification of the DMI strength, we

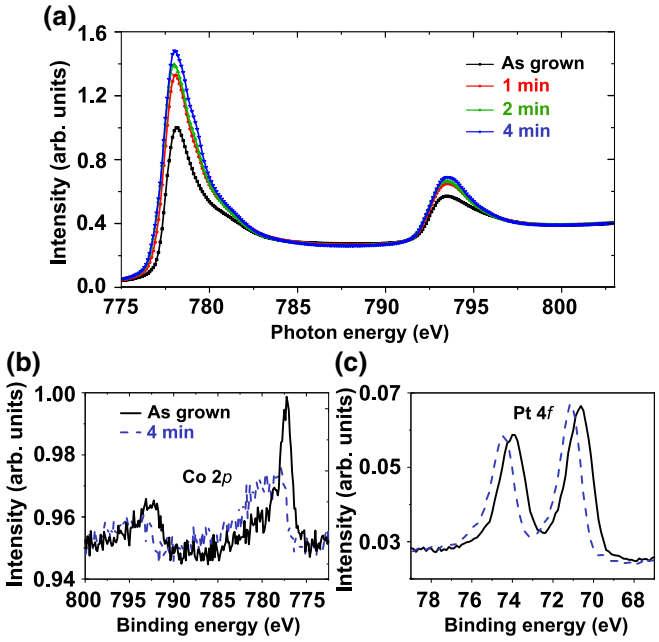

FIG. 6. (a) XAS spectra at the Co L_2 and L_3 edges as a function of biasing time. XPS spectra in the (b) Co $2p_{3/2}$ and (c) Pt $4f$ regions for an as-grown sample (solid lines) and a sample biased for 4 min (dotted lines).

conduct a thorough structural analysis to reveal the effect of the E field on the structure of the interfaces and the oxidation state of Co. This is done by conducting x-ray absorption spectroscopy (XAS), x-ray photoelectron spectroscopy (XPS), and polarized neutron reflectometry (PNR) experiments.

Figure 6 shows the XAS spectra in the energy range corresponding to the Co L_2 and L_3 edges of as-grown samples and samples biased for 1, 2, and 4 min. The known features corresponding to higher oxidation states of Co, namely satellite peaks at the L_3 edge that depend on the Co oxidation state [11,33,34], show as subtle variations in the symmetry of the main peak after biasing. However, the intensity of the L_3 peak increases significantly as a function of biasing time, which is an indication of an increase in unoccupied d levels [35] and could be correlated with a higher valence state of the Co. The increase in the Co valence inferred from XAS is confirmed by the surface analysis provided by XPS, shown in Figs. 6(b) and (c) for the as-grown sample (solid line) and a sample biased for 4 min (dotted line). A significant decrease in the intensity of the metallic Co $2p$ peaks and a shift towards higher binding energies confirm a change in the chemical environment of the Co consistent with an increase in valence. A similar correspondence between the XAS and XPS profiles has been observed in the presence of mild oxidation in $Pt/Co/AlO_x$ layers [36].

Additionally, Fig. 6(c) shows the intensity of the $4f$ peaks of Pt, where also a clear shift to higher binding energies is observed. Studies in the literature have linked a similar increase in the binding energy to an interaction with oxygen species [37], which is in agreement with the oxidation signature in the Co spectrum. No significant changes in the Hf $4f$ and O $1s$ peaks are observed (see the Supplemental Material [19]).

Further insight into the impact of the E field on the interface structure is provided by PNR measurements. This technique allows the construction of a depth profile of the magnetic and material characteristics of a system and provides a transverse characterization of the interfaces [11,12,38,39]. Figures 7(a)–7(c) show a series of high-frequency Kiessig oscillations and a second longer-period structure, corresponding to the thick SiO_2 underlayer and to thinner HfO_2,Pt, and Co layers, respectively. The splitting between the spin-up and spin-down neutron channels (R^{++} and R^{--}, respectively) is qualitatively related to the in-plane projection of the magnetization. The splitting is quantitatively presented by the spin asymmetry, defined as $\mathrm{SA} \equiv (R^{++} - R^{--})/(R^{++} + R^{--})$, which is shown in Figs. 7(d)–7(f). A model incorporating the thickness, interface roughness, magnetic scattering-length density (SLD) ρ_M, and nuclear SLD ρ_N of each of the layers is generated, and then the reflectometry of the proposed structure is calculated and compared with the experimental data. Through an iterative feedback calculation, a model is developed that accurately reproduces the experimental results. The models are fitted in parallel with coupled parameters, significantly improving the uniqueness of the converged fits.

The converged models presented in Figs. 7(g)–7(i) agree well with the expected profile, while the calculated scattering patterns, shown by solid lines in Figs. 7(a)–7(f), agree well with the experimental measurements. Unexpectedly, the nuclear structure reveals a progressive broadening of the SiO_2/Pt interface, and an increase in the Pt thickness, but little change in the Pt SLD.

The ferromagnetic signature of the Co obtained from the PNR measurements gives further insight into the mechanics of the E field, indicating a marked surface oxidation of the Co. The magnetic profile is obtained by measuring in an in-plane magnetic field (200 mT) well below $\mu_0 H_K$ of the PMA phase. Under these conditions, the as-grown sample is saturated in-plane and a proximity-induced magnetization in the Pt layer is observed. After the E-field treatment, the magnetic signal in the plane of the sample is strongly reduced and is concentrated at the Co/HfO_2 interface. This signal is the in-plane projection of the magnetization, and anisotropy effects cannot be distinguished from changes in M_s. However, this reduction can be directly related to the spin-reorientation transition evidenced by SQUID measurements, where a large PMA is present in samples biased for 2 and 4 min, in contrast to the as-grown sample, which is fully magnetized in-plane.

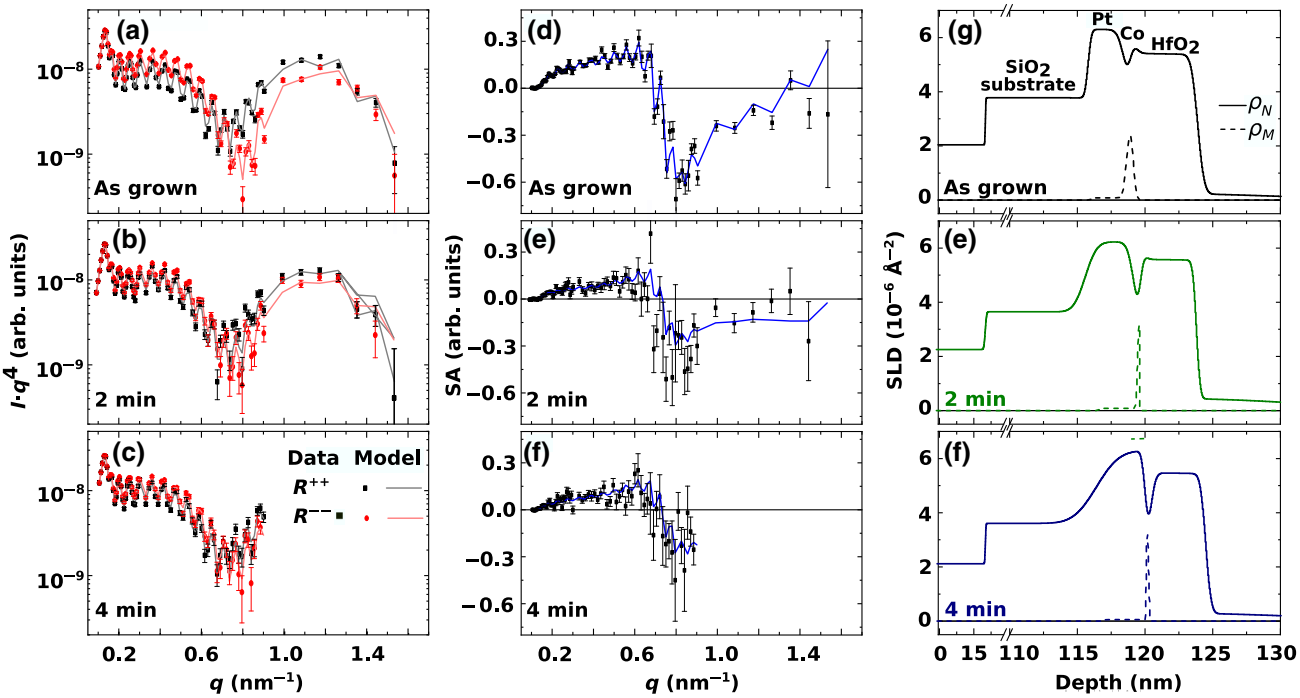

FIG. 7. (a)–(c) PNR signals R^{++} and R^{--} as a function of the wave vector, and the corresponding fitting lines; the spin asymmetry (SA) is plotted in (d)–(f). The scattering-length density (SLD), the model used to fit the experimental data, is presented in (g)–(i).

Considering the nuclear and magnetic profiles together, the fact that the initial magnetic SLD is lower than that of the bulk and the nuclear SLD is larger suggests that the as-grown Co film may be partly oxidized. If the E field were simply to induce the injection of OH^- or O^{-2} into the stack, it would decrease the magnetic SLD but would raise the nuclear SLD, which is not observed. One possibility is that the E-field treatment might inject hydrogen ions in the form of OH^-. In this context, the Pt surface could act as a catalyst and promote binding between oxygen ions and Co while inducing the irreversible anchoring of hydrogen ions to the Pt layer. This process could happen not only at the Pt/Co interface but also at the SiO_2/Pt interface, which substantially broadens after the E-field treatment. At the Co/HfO_2 interface, a stronger effect could be expected, since it is in the close vicinity of the OH^- source, the HfO_2 layer. Therefore, it is likely that the first atomic layer of Co is the one showing the highest level of oxidation. This is supported by the SLD magnetic profile, showing a magnetization in-plane component concentrated at this interface in PMA samples that could arise due to overoxidation.

Ionic motion in HfO_2 and its interplay with ambient humidity provides a possible explanation for these findings. Studies in the literature have addressed the role of water incorporation into HfO_2 exposed to air and proposed that dissociative adsorption of a water molecule at the HfO_2 surface can lead to the production of two OH^- ions [40,41]. In addition, in samples where a subsequent selective removal of the HfO_2 layer is performed, a signature of labeled OH^- ions introduced through exposure to humidity is still present, and is linked to the migration and subsequent anchoring of OH^- to the SiO_2 substrate [40]. This scenario, where preferential creation and migration of negatively charged species inside the HfO_2 layer can occur, also has a correspondence with the observed asymmetric response of the system to the E field, where no effects or reversibility are observed under positive gate voltages (see the Supplemental Material [19]). In addition, the potential anchoring of these species at the SiO_2/Pt interface could account for the large increase in the interface width that is evidenced by PNR.

V. DISCUSSION

The results presented in the previous sections reveal a complex scenario where E fields induce structural, chemical, and magnetic changes across the whole SiO_2/Pt/Co/HfO_2 multilayer, pointing to the role of ionic migration across multiple interfaces. Several studies in the literature relate E-field-induced ionic effects at a Co/oxide interface to the migration of O^{-2} ions that can bind to the Co, increasing its oxidation state [10,11,42]. Reports on Pt/NiCo/HfO_2/IL systems show reversible nonvolatile voltage effects on the magnetic properties for long biasing times between 10 and 60 min, which are attributed to

oxygen ion displacement from (to) the HfO_2 layer and subsequent oxidation (reduction) of Ni and Co as a function of the gate voltage [10]. In the present case the notion of migration of oxygen species towards the Co/HfO_2 interface is well supported by the observed partial surface oxidation of Co; however, a different scenario seems to be at play at the Pt/Co interface and even as far down as the SiO_2/Pt interface. According to the PNR analysis, ion groups, potentially including OH^- or O^{-2}, are likely to migrate towards the Pt/Co interface and into the Pt layer, inducing partial oxidation of the Co and the anchoring of neutral species that are no longer affected by E fields. This makes the E-field effect asymmetric with respect to the sign of the gate voltage and also irreversible, which is in good agreement with the experimental observations.

These important E-field-induced chemical and structural rearrangements at the Pt/Co interface are thought to be responsible for the E-field-induced reduction of the DMI. As is well known, the surface DMI is largely determined by the structure of the interfaces of the magnetic material, and the interaction with a heavy metal plays a particularly important role [43,45]. In addition, the analysis of the SLD profile leads to the conclusion that the structural changes responsible for the expansion of the Pt layer seem to take place at the SiO_2/Pt interface. The neutron SLD profile does not show marked new features at the relatively sharp Pt/Co interface, while the SiO_2/Pt interface becomes increasingly blurred after E-field exposure, which could also give rise to strain-related effects that could impact DW motion and pinning (see the Supplemental Material [19]).

Another interesting aspect to highlight is the changes taking place between the as-grown sample and the sample biased for 1 min. The reported decrease in the DMI takes place simultaneously with a marked strengthening of the PMA. The appearance of the PMA is attributed mostly to gentle oxidation of the Co at the Co/HfO_2 interface. Under- and overoxidation of Co is known to decrease PMA [36], while an optimal degree of oxidation can provide the maximum PMA, which is achieved here in the vicinity of a biasing time of 1–2 min. Recent studies [44] have shown that oxidation of the Co surface produces changes in the PMA and DMI that follow the same trend. In the present study, D is observed to decrease monotonically, showing that it is not necessarily linked to the variations in the PMA in this short-bias-time range. This points to the fact that the observed changes in the DMI are dominated by the contribution from the Pt/Co interface rather than by that at the Co/HfO_2 interface. As mentioned, an important contribution to the DMI is defined by an interface with a heavy metal with high spin-orbit coupling [44,45], and E-field-induced ion migration towards the Pt/Co interface can only produce a decrease in the DMI, unlike the simultaneous E-field-induced oxidation of the top Co interface, which can help in reaching the optimum level of oxygen content, leading to a higher PMA.

VI. CONCLUSION

We show an E-field-induced nonvolatile modification of the PMA and DMI in Pt/Co/HfO_2/IL structures. The effects observed are cumulative in time and are attributed to potential OH^- migration, recombination, and anchoring at interfaces in the presence of a negative gate voltage. IL gating allows one to permanently modify D, H_K, and M_s and to subsequently remove the IL gate for further use of the modified film in any fabrication process. Therefore, this constitutes an interesting method to achieve postgrowth PMA and DMI tuning over large scales, which can be done under ambient conditions and at room temperature. This method can make postgrowth material design possible without the demanding technical requirements of methods such as ion irradiation or plasma oxidation, which usually need complex plasma or UHV systems. This large and time-cumulative modulation of the DMI and magnetic anisotropy allows the use of E fields by IL gating not only for local control in nanodevices but also as a simple and low-cost tool for postgrowth material design.

Further developments are envisioned for this system, especially concerning the reversibility of the E-field effects, by exploring short bias times in the window between 0 and 1 min. In addition, valuable information concerning the different DMI contributions coming from the Pt/Co and Co/HfO_2 interfaces could be further explored by controlling the penetration depth of the ions. Interesting possibilities are also to be expected by exploiting the memristive capabilities of HfO_2.

ACKNOWLEDGMENTS

We gratefully acknowledge financial support from the European Union FP7 Program (ITN WALL, Grant No. 608031), from the French National Research Agency (ELECSPIN), and from the 2017 Jean d'Alembert Research Fellowship, University of Paris-Saclay Excellence Initiative. This work was also supported by a public grant overseen by the French National Research Agency (ANR) as part of the "Investissements d'Avenir" program (Labex NanoSaclay, reference ANR-10-LABX-0035). Work at UCSD and NYU was supported by Quantum-Materials for Energy Efficient Neuromorphic-Computing, an Energy Frontier Research Center funded by DOE, Office of Science, BES under Award DE-SC0019273.

L.H.D. and Y.T.L. contributed equally to this work.

[1] M. Weisheit, S. Fahler, A. Marty, Y. Souche, C. Poinsignon, and D. Givord, Electric field-induced modification of magnetism in thin-film ferromagnets, Science **315**, 349 (2007).

[2] W.-G. Wang, M. Li, S. Hageman, and C. L. Chien, Electric-field assisted switching in magnetic tunnel junctions, Nat. Mater. **11**, 64 (2012).

[3] S. S. P. Parkin, M. Hayashi, and L. Thomas, Magnetic domain-wall racetrack memory, Science **320**, 190 (2008).

[4] A. Thiaville, S. Rohart, É. Jué, V. Cros, and A. Fert, Dynamics of Dzyaloshinskii domain walls in ultrathin magnetic films, EPL (Europhys. Lett.) **100**, 57002 (2012).

[5] A. Rajanikanth, T. Hauet, F. Montaigne, S. Mangin, and S. Andrieu, Magnetic anisotropy modified by electric field in V/Fe/MgO(001)/Fe epitaxial magnetic tunnel junction, Appl. Phys. Lett. **103**, 062402 (2013).

[6] U. Bauer, L. Yao, A. J. Tan, P. Agrawal, S. Emori, H. L. Tuller, S. van Dijken, and G. S. D. Beach, Magneto-ionic control of interfacial magnetism, Nat. Mater. **14**, 174 (2015).

[7] Y. T. Liu, S. Ono, G. Agnus, J.-P. Adam, S. Jaiswal, J. Langer, B. Ocker, D. Ravelosona, and L. Herrera Diez, Electric field controlled domain wall dynamics and magnetic easy axis switching in liquid gated CoFeB/MgO films, J. Appl. Phys. **122**, 133907 (2017).

[8] A. Bernand-Mantel, L. Herrera-Diez, L. Ranno, S. Pizzini, J. Vogel, D. Givord, S. Auffret, O. Boulle, I. M. Miron, and G. Gaudin, Electric-field control of domain wall nucleation and pinning in a metallic ferromagnet, Appl. Phys. Lett. **102**, 122406 (2013).

[9] U. Bauer, S. Emori, and G. S. D. Beach, Voltage-controlled domain wall traps in ferromagnetic nanowires, Nat. Nanotechnol. **8**, 411 (2013).

[10] X. Zhou, Y. Yan, M. Jiang, B. Cui, F. Pan, and C. Song, Role of oxygen ion migration in the electrical control of magnetism in Pt/Co/Ni/HfO_2 films, J. Phys. Chem. C **120**, 1633 (2016).

[11] D. A. Gilbert, A. J. Grutter, E. Arenholz, K. Liu, B. J. Kirby, J. A. Borchers, and B. B. Maranville, Structural and magnetic depth profiles of magneto-ionic heterostructures beyond the interface limit, Nat. Commun. **7**, 12264 (2016).

[12] D. A. Gilbert, J. Olamit, R. K. Dumas, B. J. Kirby, A. J. Grutter, B. B. Maranville, E. Arenholz, J. A. Borchers, and K. Liu, Controllable positive exchange bias via redox-driven oxygen migration, Nat. Commun. **7**, 11050 (2016).

[13] A. J. Tan, M. Huang, C. O. Avci, F. Büttner, M. Mann, W. Hu, C. Mazzoli, S. Wilkins, H. L. Tuller, and G. S. D. Beach, Magneto-ionic control of magnetism using a solid-state proton pump, Nat. Mater. **18**, 35 (2019).

[14] T. Srivastava, M. Schott, R. Juge, V. Křižáková, M. Belmeguenai, Y. Roussigné, A. Bernand-Mantel, L. Ranno, S. Pizzini, S.-M. Chérif, A. Stashkevich, S. Auffret, O. Boulle, G. Gaudin, M. Chshiev, C. Baraduc, and H. Béa, Large-voltage tuning of Dzyaloshinskii-Moriya interactions: A route toward dynamic control of Skyrmion chirality, Nano Lett. **18**, 4871 (2018).

[15] T. Koyama, Y. Nakatani, J. Ieda, and D. Chiba, Electric field control of magnetic domain wall motion via modulation of the Dzyaloshinskii-Moriya interaction, Sci. Adv. **4**, eaav0265 (2018).

[16] M. Schott, A. Bernand-Mantel, L. Ranno, S. Pizzini, J. Vogel, H. Béa, C. Baraduc, S. Auffret, G. Gaudin, and D. Givord, The Skyrmion switch: Turning magnetic Skyrmion bubbles on and off with an electric field, Nano Lett. **17**, 3006 (2017).

[17] R. Mishra, F. Mahfouzi, D. Kumar, K. Cai, M. Chen, X. Qiu, N. Kioussis, and H. Yang, Electric-field control of spin accumulation direction for spin-orbit torques, Nat. Commun. **10**, 248 (2019).

[18] S. Ono, S. Seki, R. Hirahara, Y. Tominari, and J. Takeya, High-mobility, low-power, and fast-switching organic field-effect transistors with ionic liquids, Appl. Phys. Lett. **92**, 103313 (2008).

[19] See Supplemental Material at http://link.aps.org/supplemental/10.1103/PhysRevApplied.12.034005 for more details on sample growth, reversibility, and BLS, XPS, XAS, and PNR measurements, as well as for more information on the obtaining of the exchange stiffness constant A and micromagnetics simulations.

[20] M. Belmeguenai, J.-P. Adam, Y. Roussigné, S. Eimer, T. Devolder, J.-V. Kim, S. M. Cherif, A. Stashkevich, and A. Thiaville, Interfacial Dzyaloshinskii-Moriya interaction in perpendicularly magnetized Pt/Co/AlO_x ultrathin films measured by Brillouin light spectroscopy, Phys. Rev. B **91**, 180405(R) (2015).

[21] R. Soucaille, M. Belmeguenai, J. Torrejon, J.-V. Kim, T. Devolder, Y. Roussigné, S.-M. Chérif, A. A. Stashkevich, M. Hayashi, and J.-P. Adam, Probing the Dzyaloshinskii-Moriya interaction in CoFeB ultrathin films using domain wall creep and Brillouin light spectroscopy, Phys. Rev. B **94**, 104431 (2016).

[22] S.-G. Je, D.-H. Kim, S.-C. Yoo, B.-C. Min, K.-J. Lee, and S.-B. Choe, Asymmetric magnetic domain-wall motion by the Dzyaloshinskii-Moriya interaction, Phys. Rev. B **88**, 214401 (2013).

[23] H. T. Nembach, J. M. Shaw, M. Weiler, E. Jué, and T. J. Silva, Linear relation between Heisenberg exchange and interfacial Dzyaloshinskii-Moriya interaction in metal films, Nat. Phys. **11**, 825 (2015).

[24] C. A. F. Vaz, J. A. C. Bland, and G. Lauhoff, Magnetism in ultrathin film structures, Rep. Prog. Phys. **71**, 056501 (2008).

[25] T. Ha Pham, J. Vogel, J. Sampaio, M. Vaňatka, J.-C. Rojas-Sánchez, M. Bonfim, D. S. Chaves, F. Choueikani, P. Ohresser, E. Otero, A. Thiaville, and S. Pizzini, Very large domain wall velocities in Pt/Co/GdOx and Pt/Co/Gd trilayers with Dzyaloshinskii-Moriya interaction, EPL (Europhys. Lett.) **113**, 67001 (2016).

[26] C. Eyrich, W. Huttema, M. Arora, E. Montoya, F. Rashidi, C. Burrowes, B. Kardasz, E. Girt, B. Heinrich, O. N. Mryasov, M. From, and O. Karis, Exchange stiffness in thin film Co alloys, J. Appl. Phys. **111**, 07C919 (2012).

[27] K. Shahbazi, J.-V. Kim, H. T. Nembach, J. M. Shaw, A. Bischof, M. D. Rossell, V. Jeudy, T. A. Moore, and C. H. Marrows, Domain-wall motion and interfacial Dzyaloshinskii-Moriya interactions in Pt/Co/Ir(t_{Ir})/Ta multilayers, Phys. Rev. B **99**, 094409 (2019).

[28] P. J. Metaxas, J. P. Jamet, A. Mougin, M. Cormier, J. Ferré, V. Baltz, B. Rodmacq, B. Dieny, and R. L. Stamps, Creep and Flow Regimes of Magnetic Domain-Wall Motion in Ultrathin Pt/Co/Pt Films with Perpendicular Anisotropy, Phys. Rev. Lett. **99**, 217208 (2007).

[29] K. Yamada, J.-P. Jamet, Y. Nakatani, A. Mougin, A. Thiaville, T. Ono, and J. Ferré, Influence of instabilities on high-field magnetic domain wall velocity in (Co/Ni) nanostrips, Appl. Phys. Exp. **4**, 113001 (2011).

[30] L. H. Diez, M. Voto, A. Casiraghi, M. Belmeguenai, Y. Roussigné, G. Durin, A. Lamperti, R. Mantovan, V. Sluka, V. Jeudy, Y. T. Liu, A. Stashkevich, S. M. Chérif, J. Langer, B. Ocker, L. Lopez-Diaz, and D. Ravelosona, Enhancement of the Dzyaloshinskii-Moriya interaction and domain wall velocity through interface intermixing in Ta/CoFeB/MgO, Phys. Rev. B **99**, 054431 (2019).

[31] Y. Yoshimura, K.-J. Kim, T. Taniguchi, T. Tono, K. Ueda, R. Hiramatsu, T. Moriyama, K. Yamada, Y. Nakatani, and T. Ono, Soliton-like magnetic domain wall motion induced by the interfacial Dzyaloshinskii-Moriya interaction, Nat. Phys. **12**, 157 (2016).

[32] S. Moretti, M. Voto, and E. Martinez, Dynamical depinning of chiral domain walls, Phys. Rev. B **96**, 054433 (2017).

[33] T. J. Regan, H. Ohldag, C. Stamm, F. Nolting, J. Lüning, J. Stöhr, and R. L. White, Chemical effects at metal/oxide interfaces studied by x-ray-absorption spectroscopy, Phys. Rev. B **64**, 214422 (2001).

[34] B. Liu, M. M. van Schooneveld, Y.-T. Cui, J. Miyawaki, Y. Harada, T. O. Eschemann, K. P. de Jong, M. U. Delgado-Jaime, and F. M. F. de Groot, In-situ 2p3d resonant inelastic X-ray scattering tracking cobalt nanoparticle reduction, J. Phys. Chem. C **121**, 17450 (2017).

[35] C. T. Chen, Y. U. Idzerda, H.-J. Lin, N. V. Smith, G. Meigs, E. Chaban, G. H. Ho, E. Pellegrin, and F. Sette, Experimental Confirmation of the X-Ray Magnetic Circular Dichroism Sum Rules for Iron and Cobalt, Phys. Rev. Lett. **75**, 152 (1995).

[36] A. Manchon, C. Ducruet, L. Lombard, S. Auffret, B. Rodmacq, B. Dieny, S. Pizzini, J. Vogel, V. Uhlíř, M. Hochstrasser, and G. Panaccione, Analysis of oxygen induced anisotropy crossover in Pt/Co/MOx trilayers, J. Appl. Phys. **104**, 043914 (2008).

[37] C. R. Parkinson, M. Walker, and C. F. McConville, Reaction of atomic oxygen with a Pt(111) surface: Chemical and structural determination using XPS, CAICISS and LEED, Surf. Sci. **545**, 19 (2003).

[38] B. J. Kirby, P. A. Kienzle, B. B. Maranville, N. F. Berk, J. Krycka, F. Heinrich, and C. F. Majkrzak, Phase-sensitive specular neutron reflectometry for imaging the nanometer scale composition depth profile of thin-film materials, Curr. Opin. Colloid Interface Sci. **17**, 44 (2012).

[39] D. A. Gilbert, A. J. Grutter, P. D. Murray, R. V. Chopdekar, A. M. Kane, A. L. Ionin, M. S. Lee, S. R. Spurgeon, B. J. Kirby, B. B. Maranville, A. T. N'Diaye, A. Mehta, E. Arenholz, K. Liu, Y. Takamura, and J. A. Borchers, Ionic tuning of cobaltites at the nanoscale, Phys. Rev. Mater. **2**, 104402 (2018).

[40] C. Driemeier, E. P. Gusev, and I. J. R. Baumvol, Room temperature interactions of water vapor with HfO_2 films on Si, Appl. Phys. Lett. **88**, 201901 (2006).

[41] C. Driemeier, R. M. Wallace, and I. J. R. Baumvol, Oxygen species in HfO_2 films: An in situ x-ray photoelectron spectroscopy study, J. Appl. Phys. **102**, 024112 (2007).

[42] T. Hirai, T. Koyama, A. Obinata, Y. Hibino, K. Miwa, S. Ono, M. Kohda, and D. Chiba, Control of magnetic anisotropy in Pt/Co system using ionic liquid gating, Appl. Phys. Exp. **9**, 063007 (2016).

[43] H. Yang, A. Thiaville, S. Rohart, A. Fert, and M. Chshiev, Anatomy of Dzyaloshinskii-Moriya Interaction at Co/Pt Interfaces, Phys. Rev. Lett. **115**, 267210 (2015).

[44] D. de S. Chaves, F. Ajejas, V. Křižáková, J. Vogel, and S. Pizzini, Oxidation dependence of the Dzyaloshinskii-Moriya interaction in $Pt/Co/MO_x$ trilayers (M = Al or Gd), Phys. Rev. B **99**, 144404 (2019).

[45] J. Torrejon, J. Kim, J. Sinha, S. Mitani, M. Hayashi, M. Yamanouchi, and H. Ohno, Interface control of the magnetic chirality in CoFeB/MgO heterostructures with heavy-metal underlayers, Nat. Commun. **5**, 4655 (2014).

[46] P. A. Kienzle, J. Krycka, N. Patel, and I. Sahin, *Computer Software BUMPS* (University of Maryland, College Park, MD, 2011).